*Progress In Electromagnetics Research, PIER 82, 33–50, 2008*

# TRANSITION REGION EFFECTS IN TUNABLE FIBER-BASED WAVELENGTH SECTIVE DEVICES

**M. Rajabvand, F. Behnia, and M. T. Fatehi**

EE Department
Sharif University of Technology
P.O. 11365-9363, Azadi St. Tehran, Iran

**Abstract**—Tunability of fiber Bragg grating (FBG) in transition region is used to implement wavelength-selective optical intensity modulator, which superimposes a secondary low-speed data on the transit high-speed payload optical signal. Theoretical model of the device is developed and verified by measurements in the linear and nonlinear slopes of the FBG. Experiments with strong and relatively weak gratings confirm the wavelength-selectivity and stability of modulation. The fiber-based modulator is employed for optically tagging or labeling individual wavelength channels using baseband and amplitude-shift keying (ASK) modulated signals. The wavelength-selective channel labeling scheme is useful for the control and management of the optical circuits and services in WDM networks.

## 1. INTRODUCTION

In-fiber optical filtering with wavelength tuning capability is probably the most interesting feature of tunable fiber Bragg gratings (TFBG), which are widely used in fiber optic communication systems as tunable dispersion compensators, switchable add-drop filters and fiber lasers [1–12]. Usually the reflection band of the FBG is tuned to the desired wavelength channel, and optical system performance is often evaluated in terms of the relative bandwidth of signal and FBG and the tuning misalignment [13–15]. Effects of complete spectral characteristics of fiber gratings on optical signal have been studied for ultra short (picoseconds) pulses, both experimentally and numerically [16–20].

An FBG can be used not only within its rejection/transmission band, but also in transition regions of its spectrum. If the optical signal is passed through the transition band (TB) of an FBG, it experiences wavelength dependent attenuation and group delay. An example of

TB application has been reported for dynamic power equalization of erbium-doped fiber amplifier (EDFA) in [21]. In that experiment, five TFBGs have been tuned on various points in the transition regions, to provide variable attenuations for individual channels. The measured power penalty was small (about 1 dB for 2.5 Gbps data), and showed potential capability for new applications. Recently a different application area of TB has been reported in which ultra wideband (UWB) impulse radio signals are generated in the optical domain [22]. The electrical Gaussian pulses are phase modulated on an optical carrier and converted to intensity modulation via an FBG that serves as a frequency discriminator. By tuning the optical wavelength at the linear and nonlinear slopes of TB, monocycle and doublet pulses are obtained.

In this paper, we investigate transition region of FBG, and effects of its nonuniform spectral response on optical pulses passing through the filter. It is shown, analytically and experimentally, that the TB of fiber gratings can be used for wavelength-selective optical intensity modulation. We call this fiber-based technique the wavelength-selective modulation (WSM). It enables us to optically tag the routing and managing information on a multiwavelength signal in a wavelength-selective manner. Although sharp filtering properties of FBG has already been used for wavelength/packet switching in optical networks [23–31], the WSM utilizes TB for optical channel labeling/identification. We present experimental results to demonstrate the capabilities of WSM for in-fiber labeling of optical signals, which implement both subcarrier modulated ASK and direct baseband schemes.

## 2. TRANSITION REGION OF A UNIFORM FBG

To understand the behavior of FBG in transition band, we start with the amplitude transmission coefficient of a uniform FBG of length $L$, which can be shown to be [32, 33]

$$t_c = \frac{\sqrt{\kappa^2 - \hat{\sigma}^2}}{\hat{\sigma}\sinh\left(\sqrt{\kappa^2 - \hat{\sigma}^2}L\right) + j\sqrt{\kappa^2 - \hat{\sigma}^2}\cosh\left(\sqrt{\kappa^2 - \hat{\sigma}^2}L\right)} \qquad (1)$$

where $\hat{\sigma} \equiv \delta + \sigma$, $\sigma$ is a "DC" (period-averaged) coupling coefficient, the detuning $\delta$ is proportional to the frequency, and $\kappa$ is an "AC" coupling coefficient [33]. Fig. 1(a) shows the calculated power transmission coefficient ($T_c = |t_c|^2$) versus wavelength, for three different gratings with maximum reflectivity of 50%, 90% and 99.5%, which are referred to as relatively weak (RWG), strong (SG) and very strong grating

(VSG), respectively. The spectrum of uniform gratings is symmetric about the Bragg wavelength, and only upper half of the transmission spectra are shown. All FBGs have the same zero-to-zero mainlobe bandwidth of 0.8 nm. The width of TB (highlighted regions in Fig. 1), which is defined as the region between 90% and 10% of maximum reflectivity, are 0.22, 0.18, and 0.08 nm for RWG, SG, and VSG, respectively.

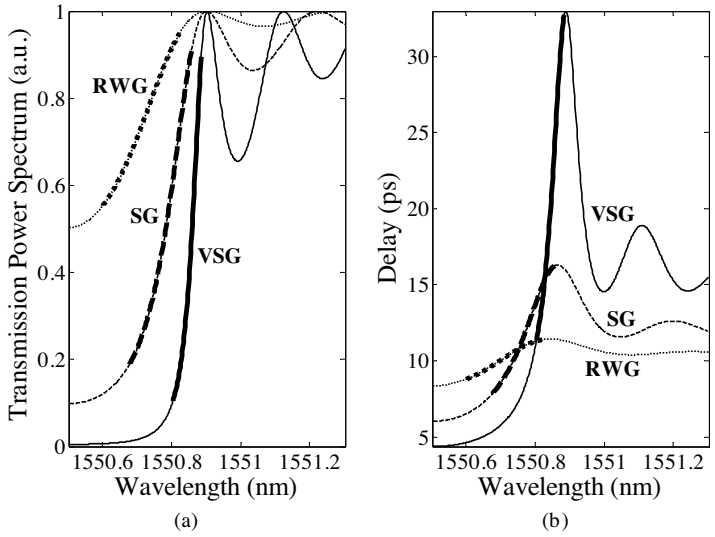


**Figure 1.** Transmission power spectra (a), and group delay (b), for three FBGs with reflectivity of 50%, 90% and 99.5%, which are referred to as relatively weak (RWG), strong (SG) and very strong grating (VSG), respectively. For the sake of symmetry only upper portion of the spectra are shown. The transition bands (highlighted regions) are defined between 90% and 10% of maximum reflectivity for each of the FBGs.

The delay time for light passed through a grating is usually given as [33]:

$$\tau_t = \frac{d\theta_t}{d\omega} = -\frac{\lambda^2}{2\pi c}\frac{d\theta_t}{d\lambda} \tag{2}$$

where $\theta_t = phase(t_c)$. Fig. 1(b) shows the delay function calculated for the three gratings of Fig. 1(a). In the transition region, $\tau_t$ is an ascending function of wavelength and its slope is higher for stronger gratings.

We calculate the spectrum of transmitted pulses by directly multiplying the $t_c$ from (1) by the input pulse spectrum, and then

take the inverse Fourier transform to obtain the output pulse shape in temporal domain. The input pulses are assumed to be transform limited Gaussian with duration of 100 and 25 ps, corresponding to data rates of 10 and 40 Gbps. The centre wavelength of laser is tuned to three different bias points: 90%, 50%, and 10% of maximum reflectivity, which is placed at the lower edge (LE), Middle (M), and upper edge (UE) of transition regions. Fig. 2 shows the pulses transmitted through the three FBGs of Fig. 1, and compare them with the case of no grating (NG), in which the optical pulses experience just a constant delay (dash-doted line). The TB of RWG is relatively broad and there are no considerable changes in pulse shape (Figs. 2(a), (b)). By sweeping the tuning wavelength of laser in transition range of the SG, the 100-ps pulse undergoes the corresponding power attenuation without any considerable change in the shape (Fig. 2(c)), however the 25-ps pulse lose its symmetry and stretches in trailing edge (Fig. 2(d)). Pulse dispersion and attenuation is more sever in passing through the VSG (Figs. 2(e), (f)), which has very narrow TB in comparison to the input pulse width. Most of the input power spectrum overlaps with reflection band or sidelobes of VSG, and results in distortion of transmitted pulses.

**Table 1.** Pulse attenuation and broadening in passing through upper edge of transition band.

| Grating strength | Relatively weak (RWG) | | Strong (SG) | | Very strong (VSG) | |
|---|---|---|---|---|---|---|
| Data rate (Gbps) | 10 | 40 | 10 | 40 | 10 | 40 |
| Loss (dB) | 0.29 | 0.75 | 0.74 | 2.25 | 1.93 | 4.53 |
| Broadening (%) | 0.8 | 2.6 | 1.9 | 16.6 | 35.5 | 37.2 |

We assume that the optical pulses are centered on the upper edge of TB, and calculate their loss and broadening in passing through three different FBGs. The results are listed in Table 1 for two data rates of 10 and 40 Gbps. The first three columns show that attenuation and nonuniformity of FBG spectra in TB do not adversely affect the transmitted-through pulses, if the grating is not very strong. Thus, it is possible to exploit the FBG in its TB without any concern about degradation of overall system performance.

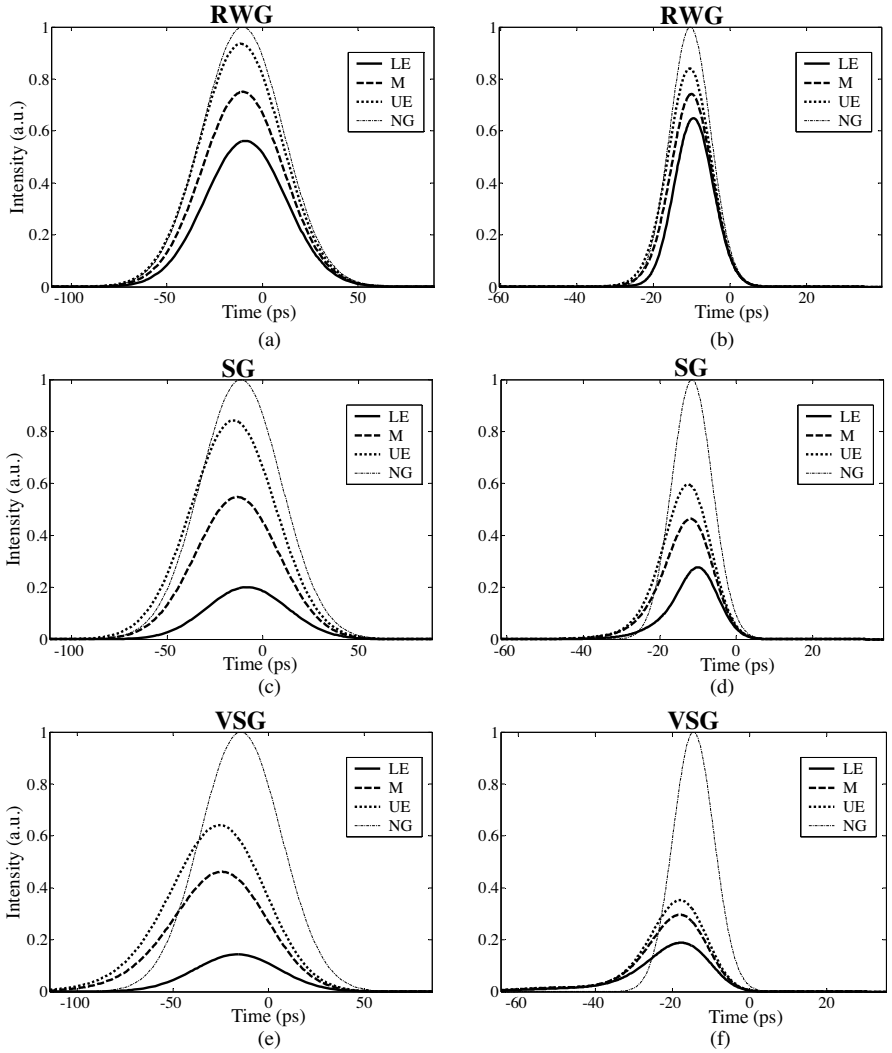


**Figure 2.** Pulses transmitted through the lower edge (LE), Middle (M), and upper edge (UE) of the transition regions in Fig. 1. The dash-dotted line represents the pulse passed through the fiber when there is no grating (NG). The input pulse is transform-limited Gaussian with duration of 100 ps (a, c, e), and 25 ps (b, d, f).

## 3. FORMULATION OF FBG-BASED OPTICAL SMALL-SIGNAL MODULATOR

Here we focus on formulation of FBG in TB and its tunability on a short wavelength interval in the vicinity of upper edge. In general the

index of refraction of fiber grating is described as a spatially varying function, $n_{eff}(z)$. The tunable FBG can be modeled by a generalized space-time variant function, $n_{eff}(z,t)$. Different tuning techniques are applied to induce strain and/or thermal variations on FBG. However, the induced refractive index variation is very slow in comparison with optical signal frequency. Therefore, we can use coupled-mode theory to obtain spectral characteristics of the FBG. Imposing a time variant strain to FBG just results in a time variant Bragg wavelength shift, that is expressed by the following simplified linear equation [34]:

$$\frac{\Delta\lambda_{Bragg}(t)}{\lambda_{Bragg}} = (1-p_e)\varepsilon_z(t) = (1-p_e)\frac{\Delta L_z(t)}{L_z} \tag{3}$$

where $\varepsilon_z(t)$ is axial strain, $p_e = 0.22$ is the effective photoelastic coefficient [35], $\Delta L_z$ is the axial displacement and $L_z$ is the stressed length. The required strain can be induced via a piezoelectric transducer (PZT). The relationship between an applied voltage $V(t)$, and the corresponding increase or decrease in thickness of PZT is expressed as: $\Delta L(t) = nd_{33}V(t)$, where $d_{33}$ is the piezoelectric charge/strain coefficient and $n$ is number of PZT layers. Thus, a linear relationship between voltage $V(t)$ and wavelength shift is obtained as follows:

$$\Delta\lambda(t)/\lambda = \eta[(1-p_e)nd_{33}/L_z]V(t) \tag{4}$$

where $\eta$ is mechanical coupling coefficient between FBG and PZT. Experimental measurements confirm this theoretical result (see, for example, [36] and [37]).

The reflected power from FBG in a specified wavelength channel $\lambda_c$ and at time $t$, relates to its reflectivity and input power as follows:

$$P_{ref}(t;\lambda_c) = R(t;\lambda_c)P_{in}(t;\lambda_c) \tag{5}$$

In general, reflectivity is a nonlinear function of wavelength but for small variations (small signal tuning), it can be approximated with a linear function in transition region.

$$R(t;\lambda_c) \cong R_{dc} \mp \frac{\partial R}{\partial\lambda}(\lambda(t)-\lambda_c) \tag{6}$$

where $R_{dc}$ is "dc" component of reflectivity at $\lambda_c$ and $\partial R/\partial\lambda$ is the slope of reflectivity function. The minus and plus signs, $\mp$, correspond to lower and upper TB, respectively. By substituting (4) and (6) into (5), the output power can be written as follows.

$$P_{ref}(t;\lambda_c) = \left[R_{dc} \mp \frac{\partial R}{\partial\lambda}\eta\gamma\lambda_c V(t)\right]P_{in}(t;\lambda_c) \tag{7}$$

where $R_{dc}$ is "dc" component of reflectivity and $\gamma = (1 - p_e)nd_{33}/L_z$ is a constant. In a similar way, we can obtain the transmitted power through FBG as:

$$P_{trans}(t;\lambda_c) = \left[T_{dc} \mp \frac{\partial T_c}{\partial \lambda}\eta\gamma\lambda_c V(t)\right] P_{in}(t;\lambda_c) \tag{8}$$

where $T_{dc}$ is "dc" component of transmitted power, and the second term shows the "ac" component which is proportional to applied voltage $V(t)$. The ac component acts like a parallel label (PL) assigned to optical channel ($\lambda_c$). Equations (7) and (8) form a linear time variant model of WSM, which analytically describe the reflected and the transmitted optical intensities as small-signal modulated signals. Using classic control methods, we can remove and modify the label via a negative feedback or feedforward method. In the feedback method, the incoming PL signal is sensed by optical tap and O/E conversion followed by a correctly tuned electrical filter. The error signal, which results from a differential amplifier, forces the WSM to remove the old label and/or replaces the new one. In the feedforward scheme, the normalized output signal of WSM can be expressed in a simple form as

$$p_0 = 1 + mv(t), \tag{9}$$

where $|v(t)| < 1$ and $m \ll 1$ is modulation index. By reverse-modulating this signal (via another WSM with a negative waveform) with the same modulation depth, the output signal is calculated as

$$\begin{aligned} p_0 &= [1 + mv(t)][1 - mv(t)] \\ &= 1 - m^2 v^2(t) \\ &\approx 1 \end{aligned} \tag{10}$$

The last result is obtained using small-signal approximation and obviously shows the PL is erased. All operations are performed in-fiber and do not require optical to electrical (O/E) conversion of the main optical signal, $P_{in}(t)$.

## 4. EXPERIMENT AND RESULTS

We experimentally demonstrated the validity of WSM model in (7) and (8), using two FBG samples with different characteristics. Their measured transmission power spectra are shown in Fig. 3. The FBG selection is in accordance with simulation results of Section 2 and do not include very strong grating. The maximum reflectivity of RWG and SG samples are 53% and 93%, and the maximum wavelengths are 1551.148 nm and 1556.080 nm, respectively.

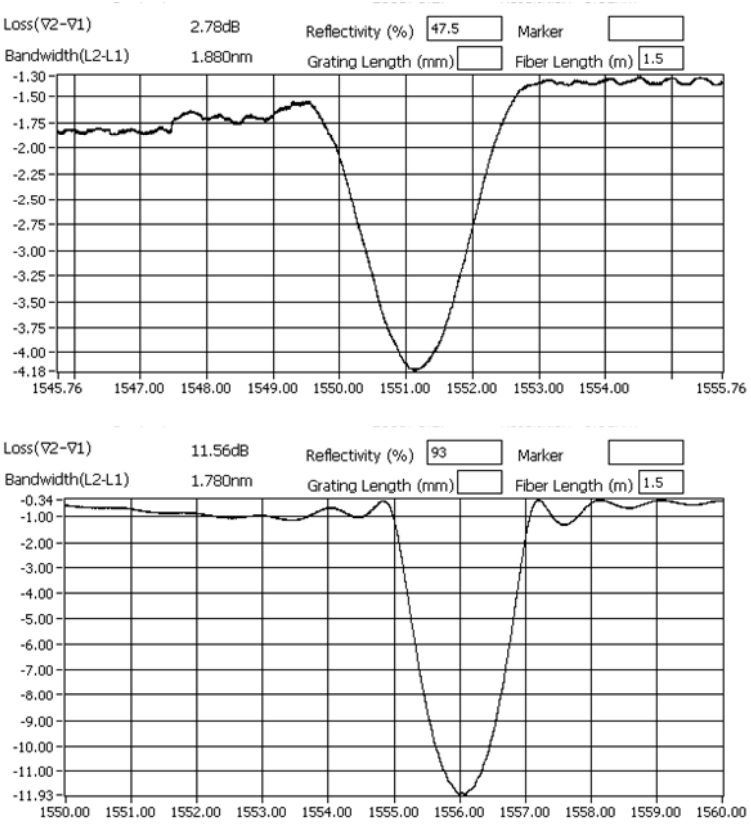


**Figure 3.** Measured transmission spectra of FBGs with reflectivity of 47.5% (upper trace) and 93% (lower trace).

The FBGs are driven by multilayer piezoelectric transducers (MLP). Very thin ceramic layers, with electrode layers in between, are combined to produce a tall stack. The electrical connections to the electrodes alternate between "+" and "−" contact strips on opposite sides of MLP (see Fig. 4(a)). Applying a low voltage across the electrodes produces a high electric field in each layer, which results large movements in axial direction. We use a MLP with dimensions of $10 \times 10 \times 36$ mm and nominal displacement of $32\mu$m @ 100 v. The measured frequency response of the MLP shows the resonance at about 45 kHz. Because of negligible mass of fiber grating (in the range of milligram), the resonance frequency is not affected by attaching the FBG to MLP.

The structure of FBG-based optical intensity modulator is shown

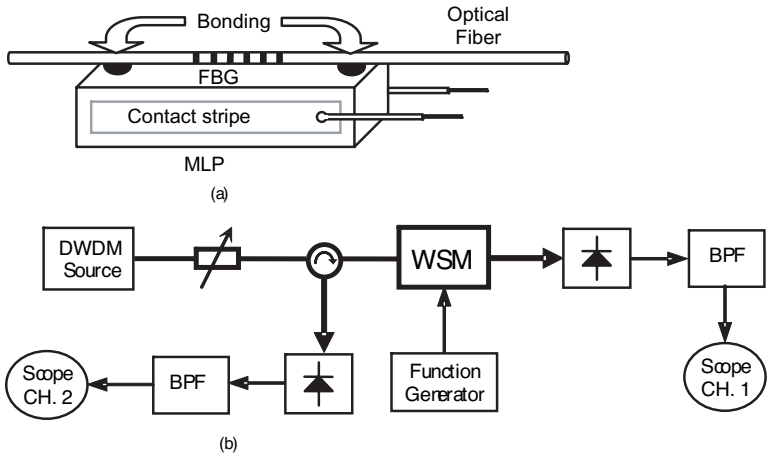


**Figure 4.** (a) Structure of Wavelength Selective Modulator (WSM) using a fiber Bragg grating and a multilayer piezoelectric transducer (MLP) and (b) Experimental setup.

in Fig. 4(a). The FBG is mounted on the MLP along the axial direction. Fiber grating is not recoated and the fiber is bare in the bonding zone. Two FBG ends are glued to the MLP such that the axial expansions of MLP directly transfer to the FBG. This configuration is designed for applying only the tensile strains on fiber grating, and compression of FBG is not considered. It requires non-negative driving voltage of the MLP ($V(t) \geq 0$), and a "DC" bias component may be added.

Fig. 4(b) shows the experimental set up of the wavelength-selective modulator (WSM). The DWDM DFB laser source consists of eight 20 mw modules with individually selectable centre wavelengths from 1551 to 1560 nm. The centre wavelength tolerance is $\pm 0.01$ nm, and the tuning range of every laser module is $\pm 1$ nm. A variable attenuator is used to control the optical power level of input light. The laser light is transmitted via a fiber optical circulator to FBG.

When an electrical signal $V(t)$ from the function generator is applied to MLP, the FBG is axially pulled from each end. The actuator displacement causes a corresponding change in the FBG length and consequently grating period and index of refraction. As a result, the Bragg wavelength fluctuates with $V(t)$, which in turn varies (modulates) the reflectivity of the FBG at the wavelength of the optical carrier. The transmitted and reflected optical power variations are detected individually using two InGaAs analogue photodiodes (PD) with responsivity of about 0.9 A/W @ 1550 nm. Two electronic filters

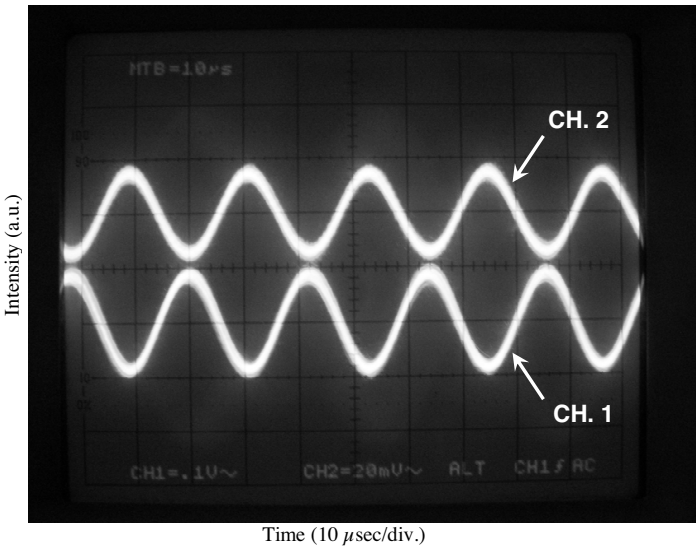


**Figure 5.** Oscilloscope traces of reflected (CH. 2) and transmitted (CH. 1) WSM signals.

(BPF) after photodetection in transmission and reflection branches are exploited to separate the WSM induced signals from noise and payload data.

Fig. 5 shows the oscilloscope traces of signals in CH. 1 and CH. 2, which measure the signal intensity transmitted through and reflected off the WSM, respectively. The phase difference of $\pi$ between the CH. 1 and CH. 2 signals is due to complementary variations of the reflected and transmitted power ($P_{ref} = P_{in} - P_{trans}$). When the optical signal wavelength is tuned near the upper edge of SG sample, on wavelength $\lambda_c = 1557.0\,\text{nm}$, it experiences 1.5 dB transmission loss. During the increasing segment of $V(t)$, the MLP displacement increases and pulls the fiber grating in length. Because of this tensile strains and the resulting increase in grating period, the Bragg wavelength shifts towards upper wavelengths, and decreases the transmission coefficient at $\lambda_c$. Thus the transmitted signal is modulated in opposite phase with respect to $V(t)$, and the reflected signal experiences a co-phase modulation.

Fig. 6 shows the measured (marked) and calculated (line) optical modulation depth versus modulating signal amplitude. The maximum Bragg wavelength shift for $V(t) \leq 1.6\,\text{v}$ is less than 0.002% and the small-signal condition is therefore satisfied. The experiment results are in good agreement with linear modulator model in (7) and (8). The

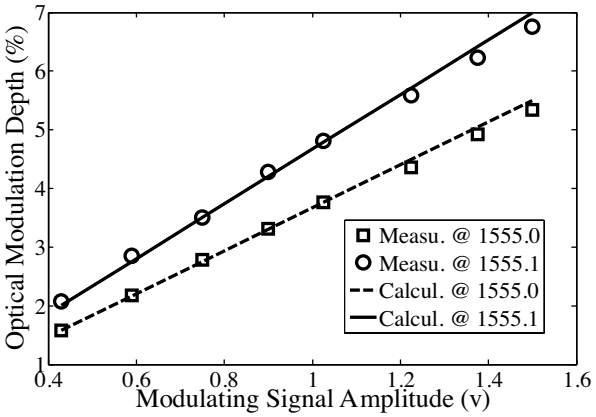


**Figure 6.** The measured (marked) and calculated (line) optical modulation depth versus modulating signal amplitude. The results are related to SG sample which is biased in the lower TB.

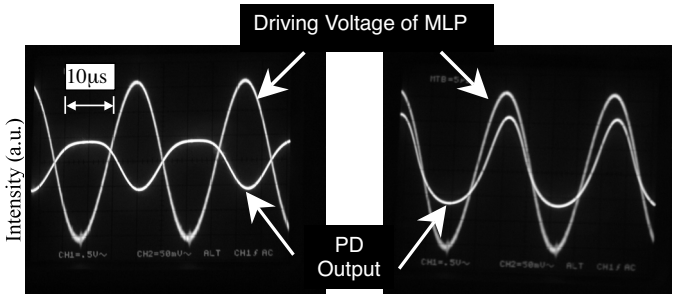


**Figure 7.** Nonlinearity effects on (a) transmitted and (b) reflected WSM signals.

modulation depth is preferably kept small (less than 10%) to avoid excessive loss of the optical signal passing through the WSM. There is a difference in the slope of the two curves that arises from different slopes of spectrum at 1555.0 and 1555.1 nm.

When amplitude of $V(t)$ is large and/or bias point ($\lambda_c$) is chosen to be in immediate neighborhood of extrema of FBG spectra, uniform ascending/descending (linearity) of transmission coefficient within tuning range fails and nonlinearity effects appear. Figs. 7(a) and (b) show the nonlinearly modulated transmitted and reflected signals, respectively. In fact, the modulation coefficient, ($\partial R/\partial\lambda$ in (7) or $\partial T_c/\partial\lambda$ in (8)), does not remain constant but it will be time variant which goes to zero at the extrema.

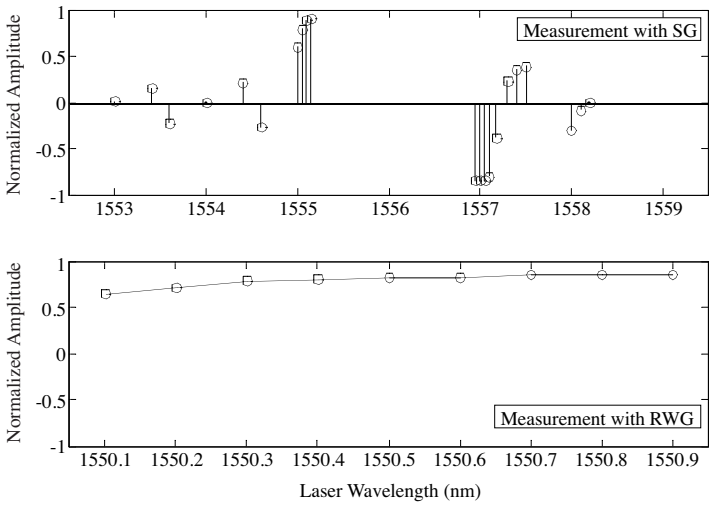


**Figure 8.** (Upper) Wavelength selectivity measurement in a broad wavelength window for a SG-based WSM, (lower) amplitude stability measured in a short wavelength window for a RWG-based WSM.

We have measured the modulation amplitude for SG and RWG samples of Fig. 3. The wavelength ranges of 1555.0∼1555.1 nm and 1557.0∼1557.1 nm are low loss ranges for SG sample and modulation amplitude is relatively high, as shown in Fig. 8 (upper). At wavelengths next to these ranges some small modulation amplitudes are seen that arise from the transfer function slope in the side lobes. The negative amplitudes are used to represent the phase difference of $\pi$ between the modulating signal and the detected PL, and correspond to negative slopes of the spectrum. Measurement with RWG sample shows stability of modulation amplitude in wavelength interval from 1550.3 nm to 1550.9 nm (Fig. 8 lower). Thus well designed fiber gratings with relatively wide transition bands and low side lobes are ideal for WSM and will be free from interference and crosstalk in multiwavelength networks.

## 5. OPTICAL CHANNEL LABELING

We use WSM to attach a label on the high-speed payload signal. In fact,$P_{in}(t)$ in (7) or (8) represents the payload signal that acts as the carrier for wavelength-selective intensity modulation. In other words, the WSM superimposes a PL, which is modeled as "ac" component in (7) or (8), on optical payload without the need for O/E conversion. The

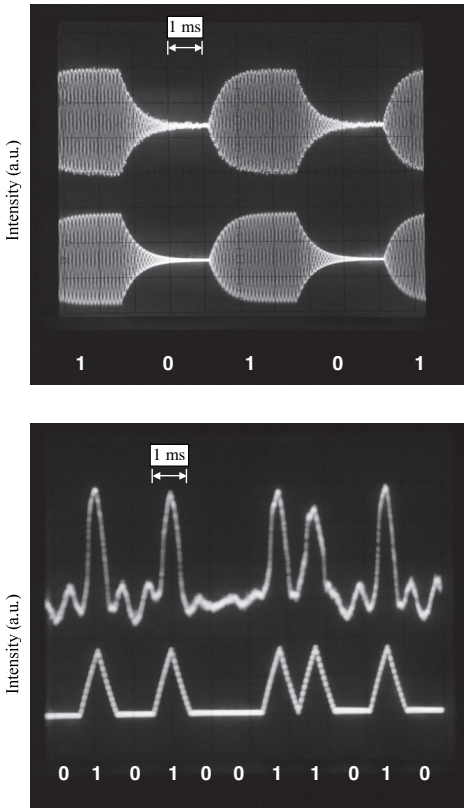


**Figure 9.** Comparisons of the input electrical label (lower traces) and optically labeled signals (upper traces), for a subcarrier modulated label (a), and a baseband label (b).

PL signal may use baseband, subcarrier modulated ASK, or any other modulation schemes (PSK, DPSK, QAM, etc). Figs. 9(a) and (b) show the results of baseband and subcarrier modulated ASK labeling using WSM. In both figures the lower traces are electrical low-speed signals, which drive the WSM, and the upper traces show the optical output after detection and filtering. In Fig. 9(a) the optical signal has been modulated with a 45 kHz subcarrier, which is ASK-modulated in a periodic "0101" pattern. Some deviations from rectangular pulse shape are seen, that are due to capacitive loading of electric drive signal by MLP. In Fig. 9(b) a baseband signal with return-to-zero (RZ) format, which is a pseudorandom bit pattern, has modulated the optical signal. Some undesired small fluctuations appear as noise, which arise from incomplete mechanical coupling between MLP and FBG. When two or

more "zero" bits are placed between "ones", the noise goes down. Since the amplitude of PL bits are always much more than the level of noise, a hard limiter with appropriate threshold can completely remove the noise from detected signal. This technique is used to detect a periodic "0101" pattern and the received noiseless labels are shown in Fig. 10. The WSM is tuned on negative and positive slopes of TB, to obtain the complementary signals of Figs. 10(a) and (b), respectively.

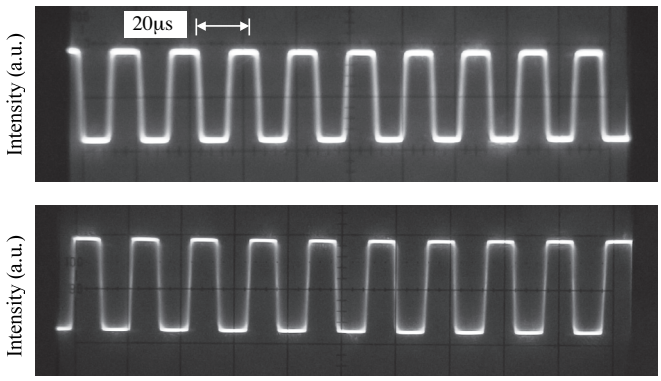


**Figure 10.** Noiseless ASK labels detected using hard limiter. (a) and (b) are induced by WSM, which is tuned in lower and upper transition band, respectively.

The maximum modulation rate of a WSM is related to dynamic behavior of piezoelectric actuator. Two major factors that determine the dynamic response of an actuator are the bandwidth and operating frequency. They are essentially limited by the mass and the electrical capacitance of actuator. Using commercially available multilayer actuators with reduced size and capacitance, we achieve the high frequency operation and broadband signaling. For example, a $2 \times 3 \times 9\,\text{mm}$ MLP with a capacitance of about $0.13\mu\text{F}$ and a resonance frequency of 135 kHz can be used to obtain similar results to those seen in Figure 9. With this optical modulator one can easily reach a rate of 20 kbps. When higher modulation rates are required, it is possible to design and implement very small actuators with higher operating frequency and bandwidth.

Due to the relatively slow speed, such a device is very suitable for quality of service (QoS) management and service level agreement (SLA) for differentiated services applications. The label can be attached to the service or circuit identifying its priority as it goes through the optical network nodes. The PLs may be replaced as needed. Also applications such as performance monitoring/control

parameters can be considered that can ride on the payload without accessing the payload.

An array of WSMs can be used for concurrent identification/labeling of multiwavelength signals in WDM network nodes. Due to wavelength selectivity of WSM, there is no need for demultiplexing and remultiplexing of the tributary wavelength channels and the WSMs are simply cascaded. This results in a lower cost, lower complexity and lower loss implementation. However, the series configuration requires appropriate electronic filtering schemes to discriminate various PLs. For example, corresponding to each channel wavelength of $\lambda_i$ there may be a specified subcarrier frequency of $f_i$. The label processor of receiver must include an electrical filter bank. After separation of the different PLs in frequency domain, they are processed individually.

## 6. CONCLUSION

In this work we have focused on tuning of FBG in transition region and its applications in optical communication systems. Results of numerical analysis of optical pulses passing through TB of various fiber gratings provided the ground work for us to investigate a fiber-based optical small-signal modulator that was formulated in Section 3. We have successfully demonstrated wavelength-selective optical intensity modulation by properly coupling the MLP to a strong and a relatively weak FBG. We have also been able to superimpose low-speed baseband and ASK modulated labels on optical signals via WSM. A series array of low cost and low loss WSMs have been developed for simultaneous optical identification/labeling of multiwavelength signals.

## REFERENCES

1. Lee, Y. J., J. Bae, K. Lee, J.-M. Jeong, and S. B. Lee, "Tunable dispersion and dispersion slope compensator using strain-chirped fiber Bragg grating," *IEEE Photon. Technol. Lett.*, Vol. 19, No. 10, 762–764, May 2007.
2. Kwon, J., S. Kim, S. Roh, and B. Lee, "Tunable dispersion slope compensator using a chirped fiber Bragg grating tuned by a fan-shaped thin metallic heat channel," *IEEE Photon. Technol. Lett.*, Vol. 18, No. 1, 118–120, Jan. 2006.
3. Xia, L., P. Shum, M. Yan, Y. Wang, and T. H. Cheng, "Tunable and switchable fiber ring laser among four wavelengths with ultranarrow wavelength spacing using a quadruple-transmission-band fiber Bragg grating filter," *IEEE Photon. Technol. Lett.*, Vol. 18, No. 19, 2038–2040, Oct. 2006.

4. Spiegelberg, C., J. Geng, Y. Hu, Y. Kaneda, S. Jiang, and N. Peyghambarian, "Low-noise narrow-line width fiber laser at 1550 nm," *J. Lightwave Technol.*, Vol. 22, No. 1, 57–62, Jan. 2004.
5. Fatehi, M. T., S. Jin, W. H. Knox, and H. Mavoori, "Controllable wavelength-selective optical cross-connect," U.S. Pat. No. 6,597,481, Jul. 2003.
6. Kim, J., J. Jung, S. Kim, and B. Lee, "Reconfigurable optical cross-connect using WDM MUX/DEMUX pair and tunable fiber Bragg gratings," *Electron. Lett.*, Vol. 36, No. 1, 67–68, Jan. 2000.
7. Singh, V., Y. Prajapati, and J. P. Saini, "Modal analysis and dispersion curves of a new unconventional Bragg waveguide using a very simple method," *Progress In Electromagnetics Research*, PIER 64, 191–204, 2006.
8. Yang, T., S. Song, H. Dong, and R. Ba, "Waveguide structures for generation of terahertz radiation by electro-optical process in GaAs and ZnGeP2 using 1.55 $\mu$m fiber laser pulses," *Progress In Electromagnetics Research Letters*, Vol. 2, 95–102, 2008.
9. Ibrahim, A.-B. M. A. and P. K. Choudhury, "Relative power distributions in omniguiding photonic band-gap fibers," *Progress In Electromagnetics Research*, PIER 72, 269–278, 2007.
10. Rostami, A. and A. Yazdanpanah-Goharrizi, "A new method for classification and identification of complex fiber Bragg grating using the genetic algorithm," *Progress In Electromagnetics Research*, PIER 75, 329–356, 2007.
11. Lim, M. H., S. C. Yeow, P. K. Choudhury, and D. Kumar, "Towards the dispersion characteristics of tapered core dielectric optical fibers," *J. of Electromagn. Waves and Appl.*, Vol. 20, No. 12, 1597–1609, 2006.
12. Gangwar, R., S. P. Singh, and N. Singh, "L-band superfluorescent fiber source," *J. of Electromagn. Waves and Appl.*, Vol. 21, No. 15, 2201–2204, 2007.
13. Gagliardi, R. M. and S. Karp, *Optical Communications*, 2nd edition, Ch. 8, Wiley, 1995.
14. Moon, N. S. and K. Kikuchi, "N*N multiwavelength optical cross-connect based on tunable fiber Bragg gratings," *J. Lightwave Technol.*, Vol. 21, No. 3, 703–718, Mar. 2003.
15. Tripathi, R., R. Gangwar, and N. Singh, "Reduction of crosstalk in wavelength division multiplexed fiber optic communication systems," *Progress In Electromagnetics Research*, PIER 77, 367–378, 2007.

16. Chen, L. R., S. D. Benjamin, P. W. E. Smith, and J. E. Sipe, "Ultrashort pulse reflection from fiber gratings: A numerical investigation," *J. Lightwave Technol.*, Vol. 15, No. 8, 1503–1512, Aug. 1997.
17. Taverner, D., D. J. Richardson, J. L. Archambault, L. Reekie, P. St. J. Russell, and D. A. Payne, "Experimental investigation of picosecond pulse reflection from fiber gratings," *Opt. Lett.*, Vol. 20, No. 3, 282–284, Feb. 1995.
18. Mishra, M. and S. Konar, "High bit rate dense dispersion managed optical communication system with distributed amplification," *Progress In Electromagnetics Research*, PIER 78, 301–320, 2008.
19. Biswas, A., "Stochastic perturbation of parabolic law optical solutions," *J. of Electromagn. Waves and Appl.*, Vol. 21, No. 11, 1479–1488, 2007.
20. Wu, J.-W. and H.-B. Bao, "Amplification, compression and shaping of picosecond super-Gaussian optical pulse using MZI-SOAs configuration," *J. of Electromagn. Waves and Appl.*, Vol. 21, No. 15, 2215–2228, 2007.
21. Liaw, S. K., K. P. Ho, and S. Chi, "Dynamic power-equalized EDFA module based on strain tunable fiber Bragg gratings," *IEEE Photon. Technol. Lett.*, Vol. 11, No. 7, 797–799, July 1990.
22. Zeng, F. and J. Yao, "Ultrawideband impulse radio signal generation using a high-speed electrooptic phase modulator and a fiber-Bragg-grating-based frequency discriminator," *IEEE Photon. Technol. Lett.*, Vol. 18, No. 19, 2062–2064, Oct. 2006.
23. Chang, G. K., J. Yu, A. Chowdhury, and Y. K. Yeo, "Optical carrier suppression and separation label-switching techniques," *J. Lightwave Technol.*, Vol. 23, No. 10, 3372–3387, Oct. 2005.
24. Zhu, Z., Z. Pan, and S. J. B. Yoo, "A compact all-optical subcarrier label-swapping system using an integrated EML for 10-Gb/s optical label-switching networks," *IEEE Photon. Technol. Lett.*, Vol. 17, No. 2, 426–428, Feb. 2005.
25. Popov, M., A. Martinez, J. Capmany, D. Pastor, P. Y. Fonjallaz, and B. Ortega, "Fiber-Bragg-grating-based device for payload and label separation in highly packed subcarrier-multiplexed optical label swapping," *IEEE Photon. Technol. Lett.*, Vol. 17, No. 11, 2445–2447, Nov. 2005.
26. Yang, J., M., Y. Jeon, J. Cao, Z. Pan, and S. J. B. Yoo, "Performance monitoring in transparent optical networks using self-monitoring optical-labels," *Electron. Lett.*, Vol. 40, No. 21, 1370–1372, 2004.

27. Lee, H. J., S. J. B Yoo, V. K. Tsui, and S. K. H. Fong, "A simple all-optical label detection and swapping technique incorporating a fiber Bragg grating filter," *IEEE Photon. Technol. Lett.*, Vol. 13, No. 6, 635–637, June 2001.
28. Hauer, M. C., J. E. McGeehan, S. Kumar, J. D. Touch, J. Bannister, E. R. Lyons, C. H. Lin, A. A. Au, H. P. Lee, D. S. Starodubov, and A. E. Willner, "Optically assisted internet routing using arrays of novel dynamically reconfigurable FBG-based correlators," *J. Lightwave Technol.*, Vol. 21, No. 11, 2765–2778, Nov. 2003.
29. Tian, C., Z. Zhang, M. Ibsen, M. R. Mokhtar, P. Petropoulos, and D. J. Richardson, "Reconfigurable all-optical packet switching based on fiber Bragg gratings," *OFC 2006 Anaheim*, Mar 5–10, 2006.
30. Tarhuni, N., M. Elmusrati, and T. Korhonen, "Multi-class optical-CDMA network using optical power control," *Progress In Electromagnetics Research*, PIER 64, 279–292, 2006.
31. Ghafoori-Fard, H., M. J. Moghimi, and A. Rostami, "Linear and nonlinear super imposed Bragg grating: A novel proposal for all-optical multi-wavelength filtering and switching," *Progress In Electromagnetics Research*, PIER 77, 243–266, 2007.
32. Kogelnik, H., "Theory of optical waveguides," *Guided-Wave Optoelectronics*, T. Tamir (ed.), Springer-Verlag, New York, 1990.
33. Erdogan, T., "Fiber grating spectra," *J. Lightwave Technol.*, Vol. 15, 1277–1294, 1997.
34. Iocco, A., H. G. Limberger, R. P. Salathe, L. A. Everall, K. E. Chisholm, J. A. R. Williams, and I. Bennion, "Bragg grating fast tunable filter for wavelength division multiplexing," *J. Lightwave Technol.*, Vol. 17, No. 7, 1217–1221, July 1999.
35. Mohammad, N., W. Szyszkowski, W. J. Zhang, E. I. Haddad, J. Zou, W. Jamroz, and R. Kruzelecky, "Analysis and development of a tunable fiber Bragg grating filter based on axial tension/compression," *J. Lightwave Technol.*, Vol. 22, No. 8, 2001–2013, Aug. 2004.
36. Inui, T., T. Komukai, and M. Nakazawa, "Highly efficient tunable fiber Bragg grating filters using multilayer piezoelectric transducers," *Optics Communications*, Vol. 190, 1–4, 2001.
37. Feng, K. M., V. Grubsky, D. S. Starodubov, J. X. Cai, A. E. Willner, and J. Feinberg, "Tunable nonlinearly-chirped fiber Bragg grating for use as a dispersion compensator with a voltage-controlled dispersion," *OFC '98 Technical Digest*, 72–74, 1998.